arXiv:1604.03378v1 [quant-ph] 12 Apr 2016

Non-Equilibrium Thermodynamics of Harmonically Trapped Bosons

Miguel Ángel García-March

ICFO Institut de Ciències Fotòniques, The Barcelona Institute of Science and Technology, Av. C.F. Gauss, 3, E-08860 Castelldefels, Spain

Thomás Fogarty

Theoretische Physik, Universität des Saarlandes, D-66123 Saarbrücken, Germany
Quantum Systems Unit, Okinawa Institute of Science and Technology Graduate University, Okinawa, 904-0495, Japan

Steve Campbell

Centre for Theoretical Atomic, Molecular, and Optical Physics, School of Mathematics and Physics, Queen's University Belfast, BT7 1NN, United Kingdom

Thomas Busch

Quantum Systems Unit, Okinawa Institute of Science and Technology Graduate University, Okinawa, 904-0495, Japan

Mauro Paternostro

Centre for Theoretical Atomic, Molecular, and Optical Physics, School of Mathematics and Physics, Queen's University Belfast, BT7 1NN, United Kingdom

Abstract. We apply the framework of non-equilibrium quantum thermodynamics to the physics of quenched small-size bosonic quantum gases in a harmonic trap. By studying the temporal behaviour of the Loschmidt echo and of the atomic density profile within the trap, which are informative of the non-equilibrium physics and the correlations among the particles, we establish a link with the statistics of (irreversible) work done on the system. This highlights interesting connections between the degree of inter-particle entanglement and the non-equilibrium thermodynamics of the system.

1. Introduction

Quantum gases offer a valuable platform for the study of quantum phenomena in interacting many-body systems. The availability of high-quality and reliable experimental control techniques and the low-level of external influences makes such systems excellent candidates for the simulation of quantum processes [1] and the exploration of the interplay between these and quantum critical behaviours.

Recent experimental progress has shown the possibility to observe non-equilibrium physics [2], which is quickly leading to the establishment of an experimental ultracold-atom framework for the exploration of complex phenomena, such as many-body localisation [3]. In particular, this framework can be used to test the recently developed ideas for the finite-time thermodynamics of closed quantum systems [4], which include tools for the quantification of thermodynamically relevant quantities, such as work and entropy, after a finite-time, non-equilibrium quantum quench. To date, this powerful formalism of non-equilibrium quantum thermodynamics has found only limited experimental validation and has been mostly applied to nuclear magnetic resonance settings [5]. However, notwithstanding the exquisite control available over such systems, they are hard to scale and offer only few possibilities for the inclusion of many-body effects. On the contrary, ultracold atomic gases offer solutions for both of these issues and it is therefore only natural to explore the features of finite-time thermodynamics in quantum gases of interacting particles.

To this aim we will in the following study the connections between the phenomenology of non-equilibrium quantum gases and finite-time thermodynamics. We consider small-size gases of interacting bosonic atoms, and apply paradigmatic perturbations to the equilibrium configuration of the gas. In particular, we focus on the ground state of interacting, harmonically trapped bosonic atoms in one dimension, and subject it to a sudden quench of the Hamiltonian parameters. Such a perturbation, which has been recently explored to characterise the occurrence of Anderson's orthogonality catastrophe [6, 7, 8], embodies the paradigm of a non-equilibrium process and has been shown to capture perfectly the complexity arising from quantum many-body effects in quantum spin systems [9]. In Ref. [10], the case of a fermionic system was addressed and developed, and the study of the statistics of work in bosonic Josephson junctions was presented in Ref. [11].

We will show the existence of a link between the average (irreversible) work done on a system of a few trapped atoms subjected to the above-mentioned quenches and the relevant figures of merit in the physics of ultracold atoms, such as the von Neumann entropy and the atomic density profile, which give information on the correlations established among the constituents of the gas under scrutiny. Our work paves the way for the investigation of larger gases subjected to a quench, a situation of great theoretical interest and experimental relevance [2].

The paper is organised as follows. In Section 2 we provide a brief introduction to non-equilibrium quantum thermodynamics, focussing in particular on the consequences

arising from a sudden quench. This formal framework is then applied in Sections 3-5 to a number of relevant physical instances of small-size low-dimensional quantum gases subjected to the quench of their Hamiltonian parameters. Finally, Section 6 draws our conclusions, while a set of technical considerations and details are presented in the Appendices.

2. Non-equilibrium thermodynamics of quantum quenches

In the following we will first briefly summarise the key notions of finite-time thermodynamics in closed quantum systems. For this we consider a system whose Hamiltonian, $\mathcal{H}$, depends on an externally controlled, time-dependent *work parameter* λ_t. The system is assumed to be in contact with a bath at inverse temperature β for a time long enough to have reached equilibrium. At $t = 0$, the system is detached from the reservoir and its energy is changed by modifying the value of the work parameter from λ_0 to λ_τ. The evolution is accounted for by the unitary propagator U_τ. As the system is detached from the surrounding world, such a change of energy can only be interpreted as work done on/by the system, which can be characterised by introducing the work probability distribution [4]

$$P(W) = \sum_{n,M} p(n, M)\delta\left[W - (E'_M - E_n)\right]. \tag{1}$$

Here E_n (E'_M) is the nth (M^{th}) eigenvalue of the associated eigenstate $|n\rangle$ ($|M\rangle$), of the initial (final) Hamiltonian. Moreover, $p(n, M) = \text{Tr}[|M\rangle \langle M| U_\tau |n\rangle \langle n| \rho_s |n\rangle \langle n| U_\tau^\dagger]$ is the joint probability of finding the system in $|n\rangle$ at time $t = 0$ and in state $|M\rangle$ at time τ, after the evolution by the time-propagator U_τ. Obviously, such a joint probability can be decomposed as $p(n, M) = p_n^0\, p_{M|n}^\tau$, where p_n^0 is the probability that the system is found in state $|n\rangle$ at time $t = 0$ and $p_{M|n}^\tau$ is the conditional probability to find the system in $|M\rangle$ at time τ if it was initially in $|n\rangle$. Therefore, $P(W)$ contains information about the statistics of the initial state and the fluctuations arising from quantum dynamics and measurement statistics. The characteristic function of the work probability distribution of $P(W)$ is defined as [4]

$$\chi(u, \tau) = \int dW e^{iuW} P(W) = \text{Tr}[U_\tau^\dagger e^{iu\mathcal{H}(\tau)} U_\tau e^{-iu\mathcal{H}(0)} \rho_{\text{eq}}^0], \tag{2}$$

with ρ_{eq}^0 being the initial equilibrium state of the system and $\mathcal{H}(t)$ the Hamiltonian of the system when the work parameter takes the value λ_t.

For a quasistatic process, the change in free energy ΔF of the system is equal to the average work done on/by it. The former can be written as $\Delta F = \Delta E - \Delta S/\beta$ with ΔE being the change in energy of the system and ΔS the corresponding entropy variation. On the other hand, if the process under consideration is fast (i.e. not quasistatic), then the relation $\langle W\rangle \geq \Delta F$ holds, accounting for the fact that part of the work performed on/by the system is *dissipated* due to the abrupt nature of the transformation. By introducing the standard definition of non-equilibrium entropy production

$$\langle \Sigma\rangle = \Delta S - \beta\langle Q\rangle, \tag{3}$$

where $\langle Q \rangle$ is the average heat exchanged with the environment, we find for a closed, unitarily evolving system

$$\langle \Sigma \rangle = \beta(\langle W \rangle - \Delta F). \tag{4}$$

This allows to quantify the irreversible nature of a given process in terms of the discrepancy between ΔF and $\langle W \rangle$. The definition of $\langle \Sigma \rangle$ allows for the consideration of the so-called irreversible work

$$\langle W_{\rm irr} \rangle = \langle W \rangle - \Delta F, \tag{5}$$

which gives an indication of the average irreversible work produced during the quenched dynamics and will be extensively used in this paper. A general approach to irreversible entropy in open quantum systems (including non-equilibrium ones) can be found in Ref. [12], while a different quantifier which is based on the use of adiabatic transformations (rather than the implicit isothermal ones considered here) has been proposed in Ref. [16].

A very useful lower bound to the non-equilibrium entropy production, $\langle \Sigma \rangle$, can be based on the unitarily invariant Bures angle (see Ref. [17]). For arbitrary density matrices $\rho_{1,2}$, the Bures angle is defined as $\mathcal{B} = \arccos\left(\sqrt{F(\rho_1, \rho_2)}\right)$ with $F(\rho_1, \rho_2)$ the fidelity between the two states. Using this one finds

$$\langle \Sigma \rangle \geq \langle \Sigma \rangle_B = \frac{8}{\pi^2} \mathcal{B}^2_{\rm eq}(\tau), \tag{6}$$

where $\mathcal{B}_{\rm eq}(\tau) = \arccos\left(\sqrt{F(\rho^\tau_{\rm eq}, \rho_\tau)}\right)$ is the Bures angle between the non-equilibrium state ρ_τ of a closed quantum system, and its equilibrium version $\rho^\tau_{\rm eq}$. Eq. (6) defines a thermodynamic distance that is valid arbitrarily far from equilibrium, and can thus be used to characterise the departure from equilibrium following an arbitrary driving process.

In this work we are interested in examining the dynamics of a cold atomic system after a sudden quench. For this we will be exploiting the fact that we start from the ground state of a given system and its state remains pure throughout the whole dynamics, which allows for significant simplifications in calculating the key quantities. We will use the spectral decomposition of the initial and final Hamiltonians of the system $\mathcal{H}_\alpha = \sum_j E^\alpha_j \left|\psi^\alpha_j\right\rangle \left\langle\psi^\alpha_j\right|$ with $\alpha = I$ ($\alpha = F$) denoting the initial (final) Hamiltonian operator. Here E^α_j is the $j^{\rm th}$ eigenvalue of $\mathcal{H}_\alpha$ with associated eigenstate $\left|\psi^\alpha_j\right\rangle$.

One key figure of merit is the Loschmidt echo (LE), which is defined as

$$\mathcal{L}(t) = |\left\langle\Psi_0\right| e^{i\mathcal{H}_F t} e^{-i\mathcal{H}_I t} \left|\Psi_0\right\rangle|^2 = \left|\sum_n e^{i(E^F_n - E^I_0)t} \langle\psi^I_0|\psi^F_n\rangle^2\right|^2, \tag{7}$$

and we have assumed that the initial state of the system $|\Psi_0\rangle$ coincides with the ground state $\left|\psi^I_0\right\rangle$ of $\mathcal{H}_I$. The LE is closely related to the characteristic function of the probability distribution of the work done on/by the system upon subjecting it to the quench considered here. In fact, for a sudden quench we have that $U_\tau = \mathbb{1}$ with $\mathbb{1}$ the identity operator in the Hilbert space of the system, and thus $\chi(u, \tau) \equiv$

$\chi(\tau) = \mathrm{Tr}[e^{iu\mathcal{H}(\tau)}e^{-iu\mathcal{H}(0)}\rho^0_{\mathrm{eq}}]$. Here, we are taking $\rho^0_{\mathrm{eq}} = \left|\psi^I_0\right\rangle\left\langle\psi^I_0\right|$ and, by using the identifications $\mathcal{H}(0) = \mathcal{H}_I$ and $\mathcal{H}(\tau) = \mathcal{H}_F$, we find $\mathcal{L}(t) = |\chi(u,t)|^2$ with

$$\chi(t) = \left\langle\psi^I_0\right| e^{i\mathcal{H}_F t}e^{-i\mathcal{H}_I t}\left|\psi^I_0\right\rangle = \sum_j e^{i(E^F_j - E^I_0)t}|\langle\psi^I_0|\psi^F_j\rangle|^2. \tag{8}$$

From this we find the average work

$$\langle W\rangle = -i\partial_t\chi(t)|_{t=0} = \sum_j (E^F_j - E^I_0)|\langle\psi^I_0|\psi^F_j\rangle|^2, \tag{9}$$

while from the definition of irreversible entropy production Eq. (4), we can introduce a quantifier of the dissipated work arising from the non-quasistatic nature of the quench.

3. Single trapped atom

Let us start by considering the simplest possible scenario of a harmonically trapped single atom in one dimension. The Hamiltonian of the system reads

$$\mathcal{H} = -\frac{\hbar^2}{2m}\partial_x^2 + \frac{1}{2}m\omega_1^2 x^2 \tag{10}$$

with m the mass of the particle and ω_1 the frequency of the trapping potential. In the following we will consider a quench in the trapping potential frequency $\omega_1 \to \omega_2$ and, in order to simplify our notation, we rescale the position of the particle with respect to the ground state length $a_{\mathrm{ho}} = \sqrt{\hbar/m\omega_2}$, and its energy with respect to $\hbar\omega_2$. The dimensionless initial Hamiltonian $\tilde{\mathcal{H}} = \mathcal{H}/(\hbar\omega_2)$ of the system then reads

$$\tilde{\mathcal{H}}^I = -\frac{1}{2}\partial_{\tilde{x}}^2 + \frac{\tilde{x}^2}{2\epsilon^2} \tag{11}$$

where $\tilde{x} = x/a_{\mathrm{ho}}$ and $\epsilon = \omega_2/\omega_1$.

The results presented in this section are closely related to those presented in Refs. [10, 17]. However an explicit re-examination of these calculations will be useful for relating the upcoming sections. To calculate any of the above quantities requires determining the overlap between the initial (ground) state and the eigenstates of $\tilde{\mathcal{H}}^F = -\frac{1}{2}\partial_{\tilde{x}}^2 + \frac{\tilde{x}^2}{2}$ [cf. Eq. (9)] which in this case can be done using the wavefunctions

$$\psi^I_0(\tilde{x}) = \sqrt[4]{\frac{1}{\pi\epsilon}}e^{-\frac{1}{2\epsilon}\tilde{x}^2} \quad \text{and} \quad \psi^F_n(\tilde{x}) = \sqrt[4]{\frac{1}{\pi}}\frac{e^{-\frac{1}{2}\tilde{x}^2}}{\sqrt{2^n n!}}H_n(\tilde{x}), \tag{12}$$

with the associated energies $E^I_0 = 1/(2\epsilon)$ and $E^F_n = (n + 1/2)$, and where $H_n(y)$ is the Hermite polynomial of order n and argument y. Exploiting the fact that $\langle\psi^I_0\left|\psi^F_{2k+1}\right\rangle = 0$ ($k \in \mathbb{Z}$), we find

$$\langle\psi^I_0|\psi^F_n\rangle = \left(\frac{2\sqrt{\epsilon}}{n!(\epsilon+1)}\right)^{\frac{1}{2}}\left(\frac{\epsilon-1}{\epsilon+1}\right)^{\frac{n}{2}}(n-1)!!, \tag{13}$$

which is valid only for even values of n and directly leads to

$$\mathcal{L}(t) = \frac{2\epsilon}{\sqrt{[2\epsilon\cos(\omega_2 t)]^2 + [(1+\epsilon^2)\sin(\omega_2 t)]^2}}, \tag{14}$$

$$\langle W\rangle = \frac{\epsilon^2 - 1}{4\epsilon}. \tag{15}$$

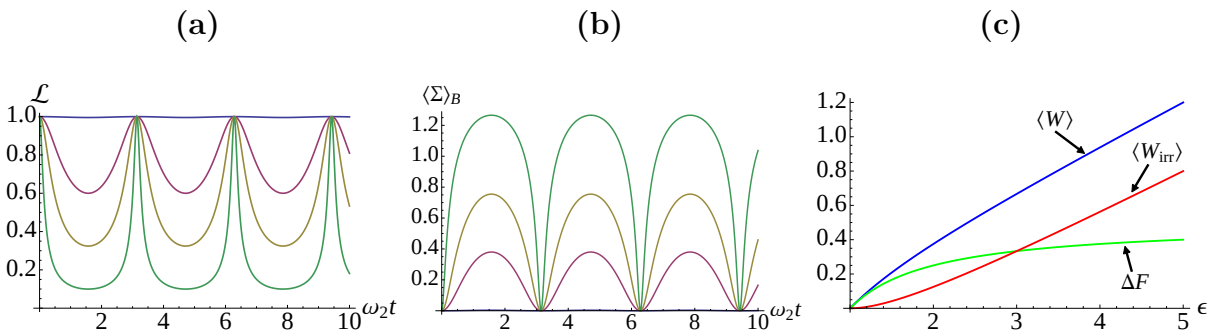

Figure 1. **(a)** The LE for a single trapped particle for increasingly large quenches $\epsilon = 1.1,\ 3,\ 6,\ 20$ (top to bottom). **(b)** Lower bound on the irreversible entropy produced by a sudden quench of the trap frequency with $\epsilon = 1.1,\ 3,\ 6,\ 20$ (bottom to top). **(c)** Average work (blue), irreversible work (red) and free energy (green) for a single trapped particle.

Note that the average work is dimensionless in our chosen units. As our system is pure, the free energy difference is simply the difference between the initial and final ground state energies, $\Delta F = \frac{1}{2\epsilon}(\epsilon - 1)$, and thus

$$\langle W_{\rm irr}\rangle = \frac{(\epsilon-1)^2}{4\epsilon}. \tag{16}$$

The lower bound of the entropy produced dynamically is given by

$$\langle\Sigma\rangle_B = \frac{8}{\pi^2}\left[\arccos\frac{2\sqrt{\epsilon}}{\sqrt[4]{(1-\epsilon)^4+(1+\epsilon)^4-2(1-\epsilon^2)^2\cos(2\omega_2 t)}}\right]^2. \tag{17}$$

In Fig. 1 we show the behaviour of these quantities for different representative values of the quench. Examining panels **(a)** and **(b)** we see an oscillating pattern stemming from the harmonic oscillator dynamics and find that the behaviour of the lower bound on the irreversible entropy is strongly correlated with the behaviour of the LE. Its value at a given time grows with the strength of the quench as a consequence of the fact that, as ϵ grows, the ground state of $\tilde{\mathcal{H}}_F$ becomes increasingly different from $\left|\psi_0^I\right\rangle$. When examined against time, we find that the maximum entropy production is achieved in correspondence with the minimum value of $\mathcal{L}(t)$. At this time, the state of the system is as different as possible from the the initial one, which coincides with the maximum irreversible entropy generated by the dynamical process undergone by the system. In Fig. 1 **(c)** we show the behavior of the average work, irreversible work and the free energy against the strength of the quench. While, naturally, all the quantities grow with increasingly large quenching strengths, $\langle W_{\rm irr}\rangle$ grows much more significantly than ΔF, precisely inline with the increasingly large maxima attained in the entropy produced for larger quenches.

4. Trapped molecule

We now move to examining the effect of particle interactions in the phenomenology of finite-time thermodynamics. For this we consider two bosonic atoms of equal mass m, jointly trapped in a harmonic potential of frequency ω_1 and then quench the trap frequency to ω_2, as before. The Hamiltonian model of the system scaled in the same way as in Eq. (11) reads

$$\mathcal{H}^{I,F} = \sum_{j=1,2} \left[-\frac{1}{2}\partial^2_{\tilde{x}_j} + \frac{\tilde{x}_j^2}{2}\frac{\omega_k^2}{\omega_2^2} \right] + g\delta(|\tilde{x}_1 - \tilde{x}_2|). \tag{18}$$

This corresponds to the initial Hamiltonian for $k = 1$ the the final for $k = 2$. The parameter g is the coupling constant, which accounts for the strength of the contact potential $g\delta(|\tilde{x}_1 - \tilde{x}_2|)$, which approximates the boson-boson interaction in the limit of low temperatures. We will assume the interactions to be repulsive throughout this work. Note that the rescaling leads to a coupling constant in units of $a_{\rm ho}\hbar\omega_2$ and for the initial Hamiltonian this again allows to define the parameter $\epsilon = \omega_2/\omega_1$.

The coupling constant can range from zero, for a non-interacting gas, to infinity, the so-called Tonks-Girardeau (TG) limit. However, we remark, in the non-interacting limit all the results of the previous section still apply. Therefore, let us start by carefully studying the TG limit, where the atoms behave as hardcore bosons and are amenable to analytic treatment. The wavefunction of the system can be split into its centre-of-mass (COM) and relative (REL) coordinates, $|\psi_n^\alpha\rangle = |\eta_n^\alpha\rangle\,|\varphi_n^\alpha\rangle$, where $|\eta_n^\alpha\rangle$ ($|\varphi_n^\alpha\rangle$) refers to the COM (REL) degree of freedom. The LE and characteristic function depend on the overlap between the initial and final wavefunctions, as before. In fact, the wavefunctions of the COM terms are precisely the same as in the single particle problem and therefore the overlap is given by Eq. (13). However, in the TG limit due to the infinite interaction each even REL state becomes degenerate with the next higher lying odd state, such that it is sufficient to work only with the odd states. The required initial and final eigenstates read

$$\begin{aligned}
\varphi_1^I(\tilde{x}) &= \left(\frac{4}{\pi}\right)^{\frac{1}{4}} \frac{1}{\epsilon}\tilde{x}e^{-\frac{1}{2\epsilon}\tilde{x}^2}, \\
\varphi_{2n+1}^F(\tilde{x}) &= \sqrt{\frac{1}{2^{2n+1}(2n+1)!}} \left(\frac{1}{\pi}\right)^{\frac{1}{4}} e^{-\frac{\tilde{x}^2}{2}} H_{2n+1}(\tilde{x}),
\end{aligned} \tag{19}$$

and have the associated energies $A_1^I = 3/2\epsilon$ and $A_{2n+1}^F = (2n + 3/2)$. We can then express the average work and the LE in terms of these functions as

$$\mathcal{L}(t) = \left| \sum_{n,p} e^{i(E_{2n}^F + A_{2p+1}^F - E_0^I - A_1^F)t} |\langle\eta_0^I|\eta_{2n}^F\rangle\langle\varphi_1^I|\varphi_{2p+1}^F\rangle|^2 \right|^2, \tag{20}$$

$$\langle W\rangle = \sum_{n,p} (E_{2n}^F + A_{2p+1}^F - E_0^I - A_1^F)|\langle\eta_0^I|\eta_{2n}^F\rangle\langle\varphi_1^I|\varphi_{2p+1}^F\rangle|^2, \tag{21}$$

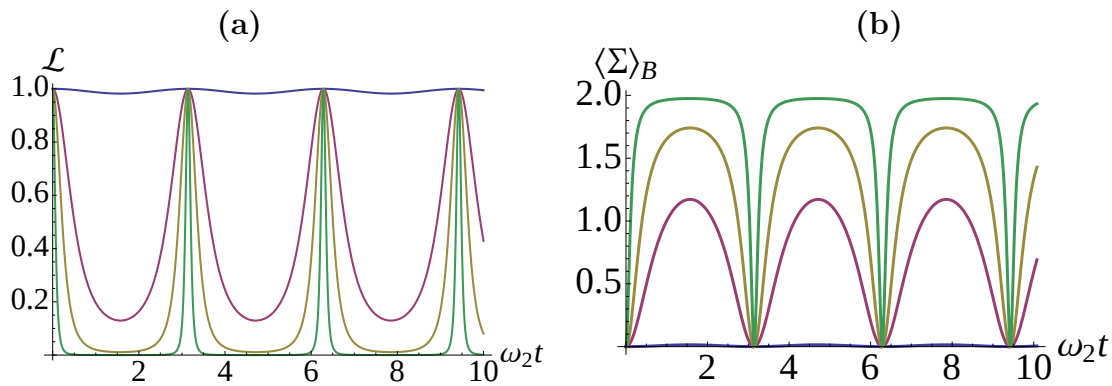

Figure 2. **(a)** Temporal behaviour of the LE of the Tonks molecule for increasingly large quenches $\epsilon = 1.1, 3, 6, 20$ (from top to bottom curve, respectively). **(b)** Lower bound on the irreversible entropy produced through the quench. We have used the same quenching amplitudes and colour code as in panel **(a)**.

with the overlap between the REL wavefunctions given by

$$\langle\varphi_1^I|\varphi_p^F\rangle = \frac{2^{\frac{p+3}{2}}\sqrt[4]{(1/\epsilon)^3}p!!}{\sqrt{2^p p!(1/\epsilon+1)^{p+2}}}\left(1-\frac{1}{\epsilon}\right)^{\frac{p-1}{2}}. \tag{22}$$

Using this expression we can calculate the LE using Eq. (20) and $\langle\Sigma\rangle_B$ using Eq. (6). The infinite sums can be evaluated explicitly, and the final expression for the average work turns out to be exactly four times the single-particle work

$$\langle W\rangle = \frac{\epsilon^2-1}{\epsilon}, \tag{23}$$

showing that in this regime work is an extensive quantity as we have performed a quench of the trap frequency for two particles [compare to Eq. (15)]‡. This can be further understood from the fact that in the TG limit the bosons behave as non-interacting fermions [10]. In Fig. 2 we show the behaviour of $\mathcal{L}(t)$ and $\langle\Sigma\rangle_B$. While the qualitative behaviour is consistent with the single particle case, we see that the effect of the interactions is to magnify these features as we now must account for many-body effects. In particular, we also see the system periodically evolves into fully orthogonal states for $\epsilon \gtrsim 6$ as the interacting two-body system can be moved further out of equilibrium.

The situation defies analytical treatment when the frequency of the trap is quenched while the interaction strength is kept finite, that is between the non-interacting and the Tonks-Girardeau limit. An informative figure of merit on the dynamics undergone by the system is provided by the von Neumann entropy (vNE) of the state of a given atom

$$S = -\mathrm{Tr}\left[\rho^j \ln \rho^j\right] \qquad (j=1,2), \tag{24}$$

where ρ^j is the reduced state of atom j. As we consider the system to be initially in the ground state, the vNE is a good measure of the entanglement established between the particles following the quench. For finite values of g, quenching the trap frequency

‡ In the Tonks limit we find the average work scales as N^2 times the single particle average work.

implies also a quench of the interaction strength between the particles and therefore the evolution of the vNE will be determined by the competition between these two mechanisms.§ The resulting non-trivial behaviour is shown in Fig. 3 for various values of the quench amplitude and the coupling strength g. For small-amplitude quenches and weakly interacting atoms (lower blue curve in Fig. 3 **(a)**) the vNE oscillates, as expected for a quench in a harmonic oscillator, with an amplitude modulation due to the interaction. At larger strengths of the quench (lower blue curve of panel **(b)**) this behaviour is strongly modified. The absolute values of the entanglement increase, as the system becomes strongly correlated, but there is no longer evidence of regular oscillations as the spectrum has become anharmonic due to the interactions. Looking at the spectral function of the out of equilibrium state, $A(\omega) = 2Re \int \chi(t) e^{i\omega t} dt$, one can identify these different excitation frequencies inherent in the evolution, see Fig. 4. The majority of the motion is governed by the quasi particle peak at the ground state energy of the quenched state $E_0^F + A_0^F$, and smaller contributions from combinations of COM and REL even states at higher energies (there are no contributions from the odd states). At larger interaction strengths the high energy peaks in the spectral function approach each other, as the system becomes doubly degenerate in the TG limit. This causes larger interference effects that are apparent in the entropy evolution (c.f. the upper red curves in Fig. 3 **(a)** and **(b)**). The periodic nature of the revivals is destroyed for the large quench of $\epsilon = 5$ due to the broadening of the high energy peaks (see inset of Figs. 4 **(c)** and **(d)**). A clear signature of interference due to the interplay from the initial value of g, and the subsequent change of it due to the quench is also manifested in the appearance of Fano-resonances in the spectral function (see all insets in Fig. 4).

To evaluate the finite-time thermodynamics of the system following the quench, we show in Fig. 5 the LE for the same parameters as used in Fig. 3. The periodic nature of the echo is visible for the small quench ($\epsilon = 2$) exhibiting breathing dynamics which are a consequence of the non-trivial energy shifts the system caused by the interaction [13, 14, 15]. In this case the high frequency oscillations are created by the trap frequency quench while the slower frequency envelope is a consequence of the interactions. For the larger quench ($\epsilon = 5$) it is clear that this beating is destroyed resulting in orthogonality and interference effects from the contributions of higher energy states. In the remainder of this section we concentrate on the behaviour of the irreversible work $\langle W_{\rm irr} \rangle$ and try to establish a connection between the amount of entanglement created between the two atoms and the degree of dissipated work achieved. To this aim, we first show in Fig. 6 the qualitative behavior of $\langle S \rangle$, $\langle W \rangle$, and $\langle W_{\rm irr} \rangle$, as a function of the inter-atomic coupling strength. Here

$$\langle S \rangle = \frac{1}{\tau} \int_0^\tau S(t) dt, \tag{25}$$

is the time-averaged vNE, with τ being a time-interval that is long enough to include many periods of oscillation. We can see that regardless of the quench amplitude $\langle W_{\rm irr} \rangle$

§ We remark that we do not examine the vNE in the Tonks limit as it is a pathological case, due to infinite value of the interaction the vNE will remain constant for all quenches.

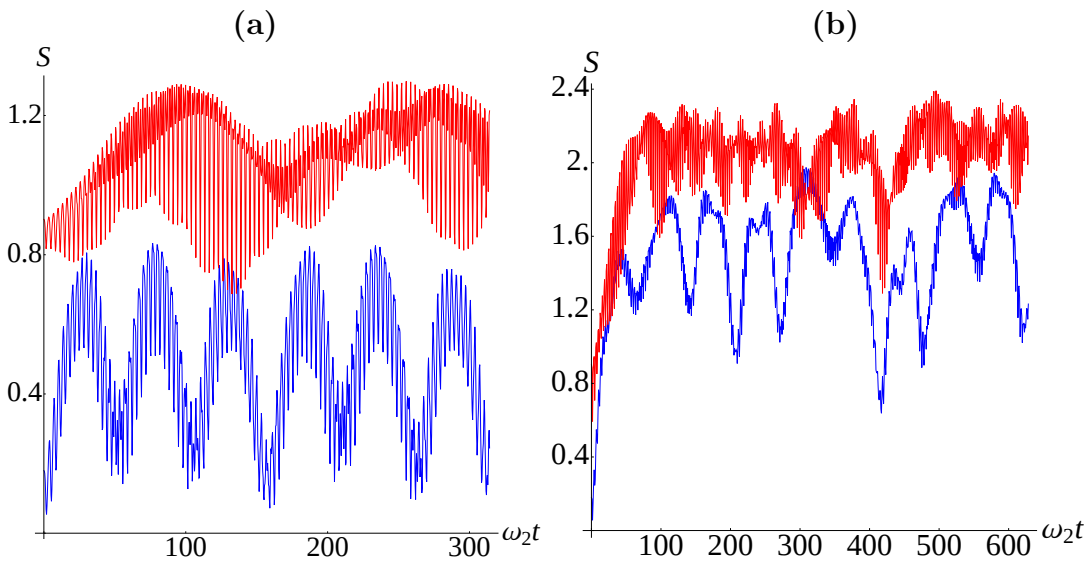

Figure 3. **(a)** Evolution of the vNE following a quench of the trap frequency against the dimensionless time $\omega_2 t$ for $\epsilon = 2$ and two values of the coupling strength. The red (blue) curve is for $g = 20$ ($g = 1$). **(b)** Same as panel **(a)** with $\epsilon = 5$.

and $\langle S \rangle$ appear to follow the same qualitative behavior as a function of the strength of the interaction. Although the establishment of a causal link between such figures of merit goes beyond the scope of this work, one can clearly see an interesting correlation that quasi-linearly relates $\langle S \rangle$ to the amount of (irreversible) work done on the system [cf. Fig. 7].

It is worth noting that a number of recent works have managed to establish a rigorous link between the appearance of correlations (both quantum and classical) and the associated thermodynamic cost [18] (albeit applying a separate formalism to the one considered here), that is complementary to our analysis. Indeed, our results suggest a significant role for thermodynamic work in the establishment of quantum correlations between the particles. Such a connection has previously been highlighted in the context of spring-like coupled bosons [19], and is here reinforced and extended, rather significantly, to the case of contact-like interactions. Our study therefore goes well beyond the paradigm of quadratic coupling addressed before and opens up the possibility of investigating systems with larger particle numbers.

5. Three trapped atoms

We now extend the Hamiltonian model addressed so far to the case of a one-dimensional mixture of two identical bosons of the same species X, whose coordinates will be indicated as x_1 and x_2, and one impurity atom of a different species Y, with coordinate y. We assume that all particles have the same mass m and are trapped with the same oscillator frequency ω. The interactions are again of contact form, characterised by the intra- and inter-species coupling constants $g_{\rm X}$ and $g_{\rm XY}$. In this situation, the

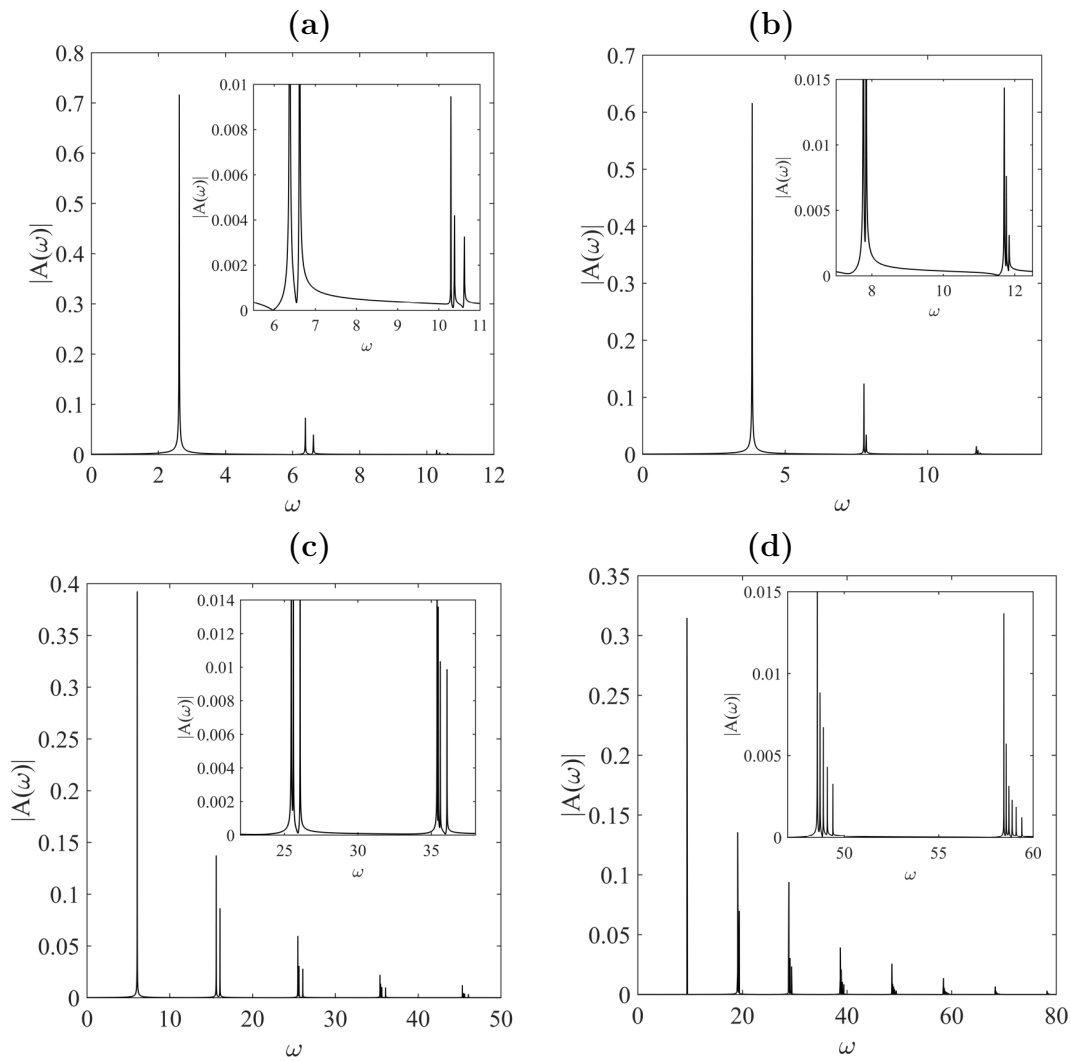

Figure 4. Spectral function for $\epsilon = 2$ with **(a)** $g = 1$ and **(b)** $g = 20$, and for the stronger quench of $\epsilon = 5$ with **(c)** $g = 1$ and **(d)** $g = 20$.

Hamiltonian reads

$$\mathcal{H} = -\frac{1}{2}\left[\sum_{j=1}^{2}\left(\partial^2_{x_j^2} - x_j^2\right) + \left(\partial^2_{y^2} - y^2\right)\right] + g_{\mathrm{X}}\delta(|x_1 - x_2|) + g_{\mathrm{XY}}\sum_{j=1}^{2}\delta(|x_j - y|), \tag{26}$$

where the dimensionless coordinates are defined by rescaling energies and coupling rates as above. Note that the eigenfunctions of Eq. (26) have to be symmetric with respect to the exchange of the X bosons, but no symmetry restriction for the interchange of the X atoms with the Y atom exists. A detailed study of the forms and properties of the eigenstates $\Psi(x_1, x_2, y)$ of Eq. (26), focusing on the degeneracies of the spectrum, is given in Appendix A.

In the following we will make use of the one-body density matrix (OBDM) that can

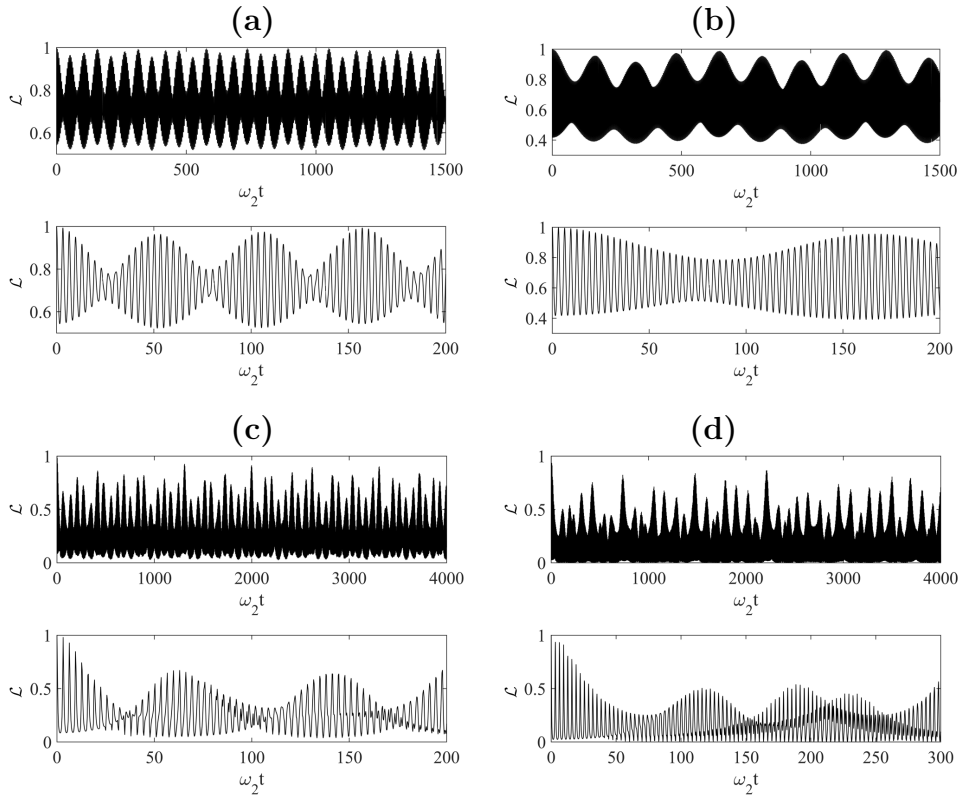

Figure 5. LE for $\epsilon = 2$ with **(a)** $g = 1$ and **(b)** $g = 20$, and for the stronger quench of $\epsilon = 5$ with **(c)** $g = 1$ and **(d)** $g = 20$. Each lower panel shows a magnified version of the evolution.

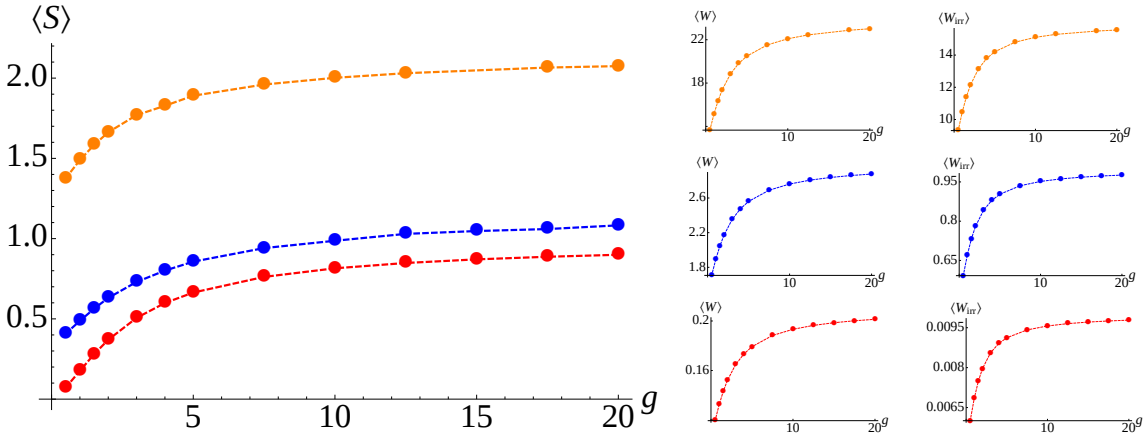

Figure 6. Average vNE (main panel), average work $\langle W \rangle$ (left column), and average irreversible work $\langle W_{\rm irr} \rangle$ (right column) following a quench of the trapping frequency against the strength of the interactions g. The red curves correspond to $\epsilon = 1.1$, the blue curves are for $\epsilon = 2$, and the orange curves are for $\epsilon = 5$. The average vNE $\langle S \rangle$ is calculated by averaging over 100 oscillations, which ensures good convergence of the numerical results.

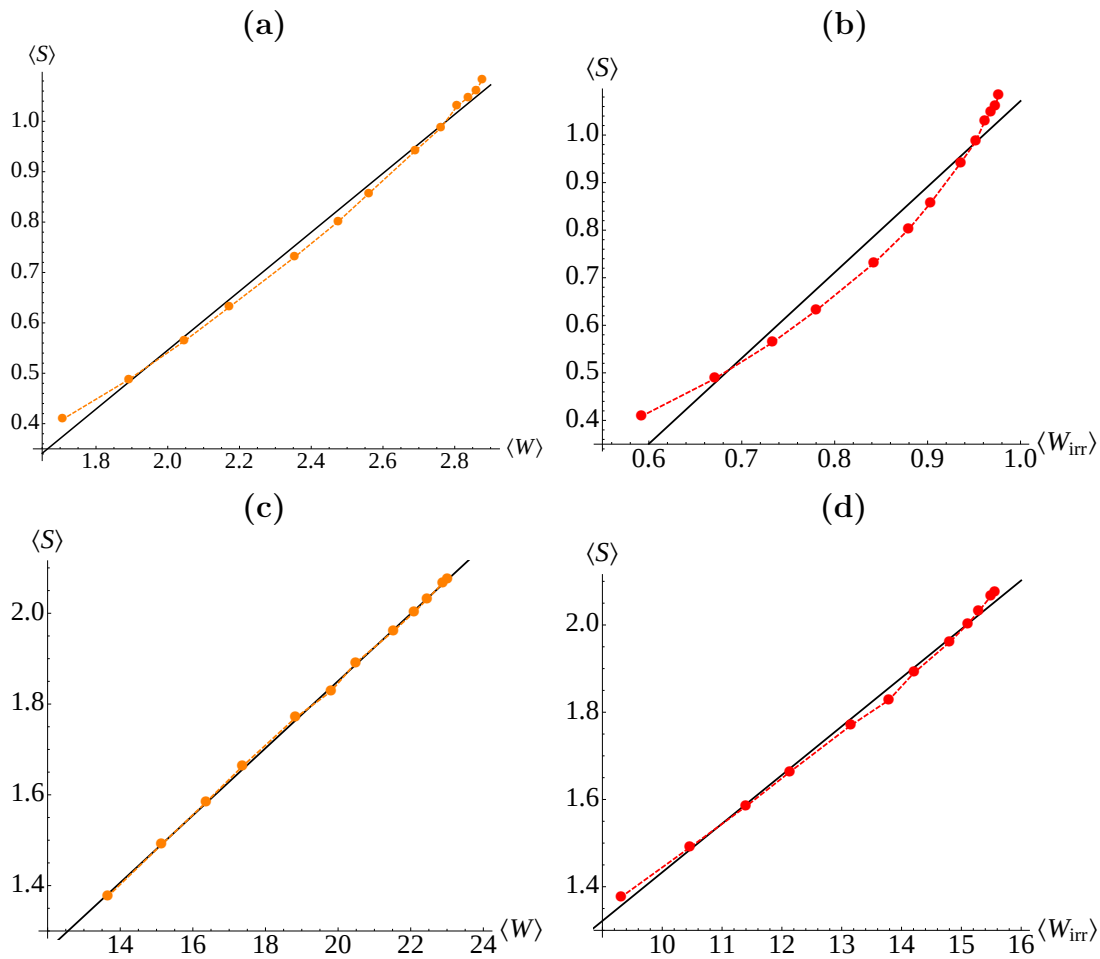

Figure 7. Time-averaged vNE vs. (irreversible) work done on the system of two trapped bosonic atoms subjected to a quench of the trapping frequency. In all panels each point represents the value taken by the pair at a set value of g. The (black) straight lines show the result of a linear fit of the data points. Panel **(a)** shows the behaviour of $\langle S\rangle$ against $\langle W\rangle$ and panel **(b)** shows the behaviour of $\langle S\rangle$ against $\langle W_{\rm irr}\rangle$ for $\epsilon = 2$. Panels **(c)** and **(d)** are for $\epsilon = 5$.

be calculated by taking the partial trace of the state of the three-particle system over two of the particles. The OBDM of one of the X atoms is

$$\rho^{\rm X}(x,x') = 2\int dx_2 dy |\Psi(x_1,x_2,y)]|^2 = \sum_k f_k^{\rm X}(x') f_k^{\rm X}(x)\lambda_k^{\rm X}, \tag{27}$$

and analogously, for the impurity atom of species Y, we have

$$\rho^{Y}(y,y') = \int dx_1 dx_2 |\Psi(x_1,x_2,y)|^2 = \sum_k f_k^{\rm Y}(y') f_k^{\rm Y}(y)\lambda_k^{\rm Y}. \tag{28}$$

Here the functions $f_k^{\rm X,Y}$ are the natural orbitals that diagonalise the OBDM in both cases with natural orbital occupations $\lambda_k^{\rm X,Y}$. Accordingly, we can also define the vNE of the state of a given atom. By calling $S^{\rm Y}$ the vNE of the reduced state of the impurity

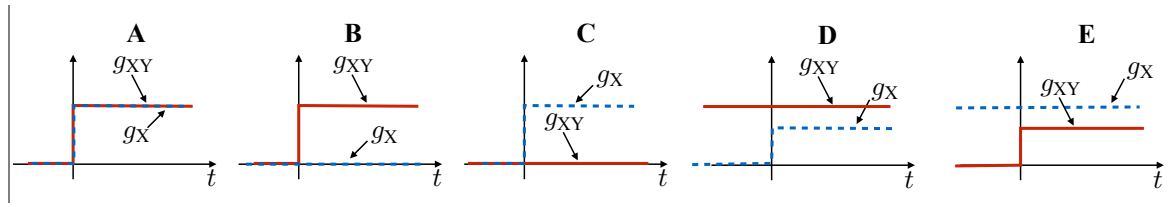

Figure 8. Sketch of the five different quenching strategies considered for the three-atom system. The quenches **D** and **E** could in principle lead to the same final values for g_X and g_{XY}.

and S^X that of *one of the atoms of species X*, we have in the notation above

$$S^{X,Y} = -\sum_k \lambda_k^{X,Y} \ln \lambda_k^{X,Y}. \tag{29}$$

Due to the presence of two coupling constants, g_X and g_{XY}, which can range between 0 and infinity, this system possesses a rich dynamics. However, if one assumes $g_X = g_{XY} = 0$ or $g_X = g_{XY} \approx \infty$ and quenches the trapping frequency, one does not obtain qualitatively different results from the one and two particle cases discussed above. Since for finite g_X or g_{XY} quenching the trapping frequency also implies a quench in the coupling constants, which significantly complicates the analysis of any results obtained, we study in the following the more accessible situation where the coupling constants are quenched directly.

5.1. Quenching protocols

Our study concentrates on five different quenches in the coupling constants given by (see also Fig. 8)

A $(g_X, g_{XY}) = (0, 0) \to (g, g)$
B $(g_X, g_{XY}) = (0, 0) \to (0, g)$
C $(g_X, g_{XY}) = (0, 0) \to (g, 0)$
D $(g_X, g_{XY}) = (0, \infty) \to (g, \infty)$
E $(g_X, g_{XY}) = (\infty, 0) \to (\infty, g)$

The energy spectra corresponding to the adiabatic version of these quenches are shown in Fig. 9. Note that these have been reported before (see e.g. Refs. [22, 23, 24]), except, to our knowledge, the panel corresponding to strategy **E**, where we show how the energy spectra changes from a situation in which g_X is large and g_{XY} is increased from zero to a large value. This corresponds to a situation in which initially there is a Tonks-Girardeau gas of two atoms, and a third distinguishable atom starts to interact with them.

The energy spectrum for the situation where both coupling constants have the same value (related to quench strategy **A**), shows the emergence of three-fold degenerate states in the limit of infinite interaction strengths. The same limit can be reached by first increasing g_{XY}, while keeping $g_X = 0$ (related to quench strategy **B**), which leads

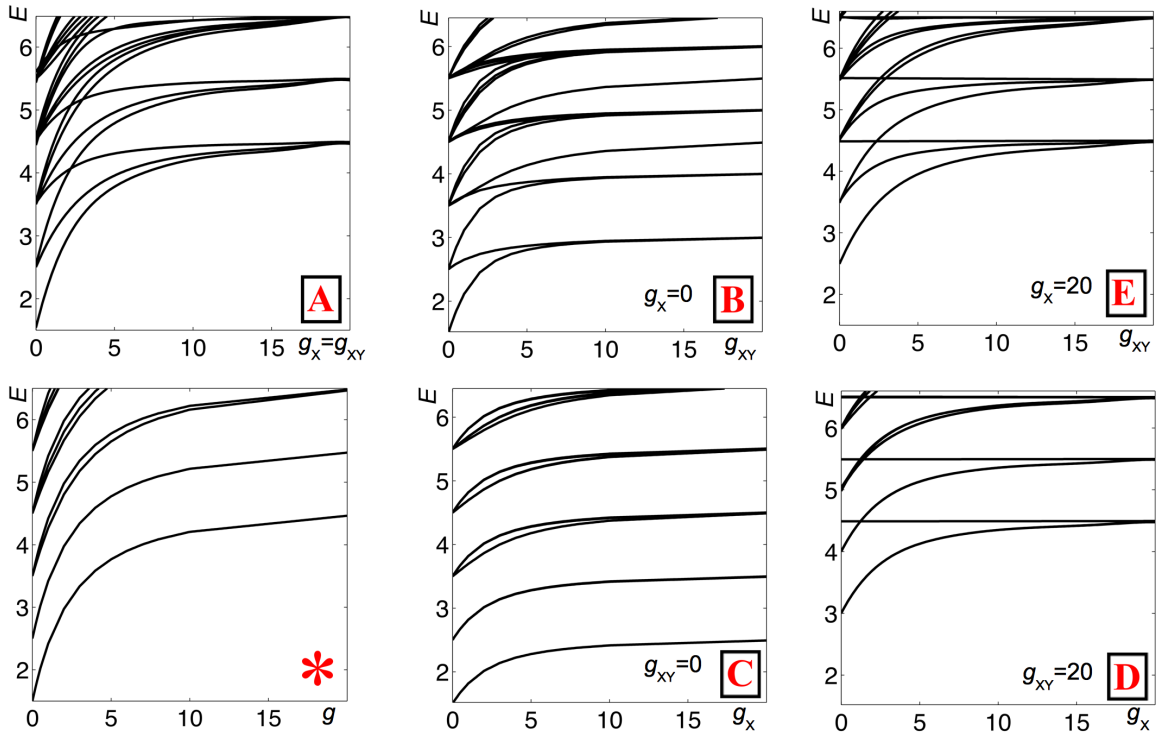

Figure 9. Energy eigenspectra for systems with different scattering symmetry requirements. The sprectra relating to quenches **A**, **B**, and **E** fix the intra-species coupling strength, g_{X}, and change the inter-species coupling strength, g_{XY}, while for the spectra **C** and **D** the opposite is the case. The situation **A**, where symmetric scattering between two of the particles is required (and absent for the scattering with the third particle) should be compared to ($*$), where the spectrum for a gas of three indistinguishable particles is shown. In this system the existence of a symmetry condition between all particles was assumed. In situation **B** all symmetry requirements are absent, and it should therefore be compared situation **C**, where only scattering with a symmetry requirement is present. Finally, in situation **D** the symmetric scattering is fixed and the scattering without the symmetry condition is varied, which should be compared to the situation **E** where the opposite is the case.

to a two-fold degeneracy at large amplitudes, and subsequently increasing g_{X} (related to strategy **D**). One can see that, for the low lying states that are important to our analysis, the two-fold degeneracy that exists for small g_{X} and large g_{XY} is transformed into the expected three-fold degeneracy when both g_{X} and g_{XY} are large. Finally, if we increase g_{X} while keeping $g_{\mathrm{XY}} = 0$ (related to strategy **B**), one simply reproduces the analytical results found in [25]. To reach the infinitely interacting limit, one must then increase g_{XY} (related to strategy **E**), where we see again that the expected three-fold degeneracy emerges in the infinitely interacting limit. From the differences between these energy spectra it is therefore clear that each quenching protocol provides different thermodynamic and density evolutions, which we will discuss below.

5.2. Themodynamic quantities

The thermodynamic consequences of the quenching processes discussed above depend on the exact form of the related energy spectra and can therefore be expected to differ. In the cases considered in strategies **A, B** and **C** the bosonic particles are initially non-interacting and in the same state. This is not the case for strategies **D** and **E**, in which many natural orbitals have non-zero occupation even before the respective quenches [26, 27, 22]. As the vNE is strongly dependent on the correlations in the initial state, we can therefore expect a different entropy evolution depending on the kind of quench. For strategy **A** the behaviour of the vNE is shown in Fig. 10 **(a)**, with panel **(b)** showing the evolution of the two largest natural orbital occupations. It is worth noting that the behaviour for both quantities is the same whether two X atoms or one X and one Y atom are traced out. This can be understood by realising that when quenching the two coupling constants to the same value, the system behaves identical to one composed of three indistinguishable atoms. It indicates that only the energy levels that both systems have in common are affected by the quench and there is no difference between the respective OBDMs. A more formal argument using group theory is presented in Appendix B.

As expected, one can also see that the entanglement increases with the amplitude of the quench and that dips appear with a periodicity close to multiples of the trapping frequency. These are more harmonic and narrower when the system is quenched into the TG regime ($g = 20$), as it can then be mapped onto non-interacting fermions. The occupations of the natural orbitals also show an oscillatory behaviour, which again is related to the trapping frequency.

In Figs. 10 **(c)** and **(d)** we show the evolution of the vNE for strategy **B**. Note that for this quench S^{X} and S^{Y} differ. Again, the vNE grows for stronger quenches, but the periodical dips are less pronounced compared to the ones observed with strategy **A**. This is not surprising, as the spectrum for this situation is denser and therefore more states contribute to the evolution, which makes perfect refocussing less likely. We omit the analysis of the evolution of the vNE for strategy **C**, as it is the same as quenching the coupling constant in a system of two atoms. Due to the absence of interaction, particle Y has only a spectator role in this case. The dynamical behaviour of the vNE for strategy **D** is shown in Figs. 10 **(e)** and **(f)**. As the interaction between the two species is already large at the beginning, the initial values of the correlations are now finite and the quench increases them to a similar level as in the cases above. Similarly, periodic dips appear again around the refocussing time of the harmonic trap. Similar considerations hold qualitatively for strategy **E**, and thus we do not explicitly discuss it here (see also [8]).

The LEs following the quenches are shown in Figs. 11 **(a)** - **(e)** and, similar to the behaviour of the vNE above, they display regular revivals, whose period moves closer to the harmonic oscillator time scale of multiples of $\omega t/\pi$ for large quench amplitudes (when the system is quenched to the TG regime). As the evolution of the LE is independent

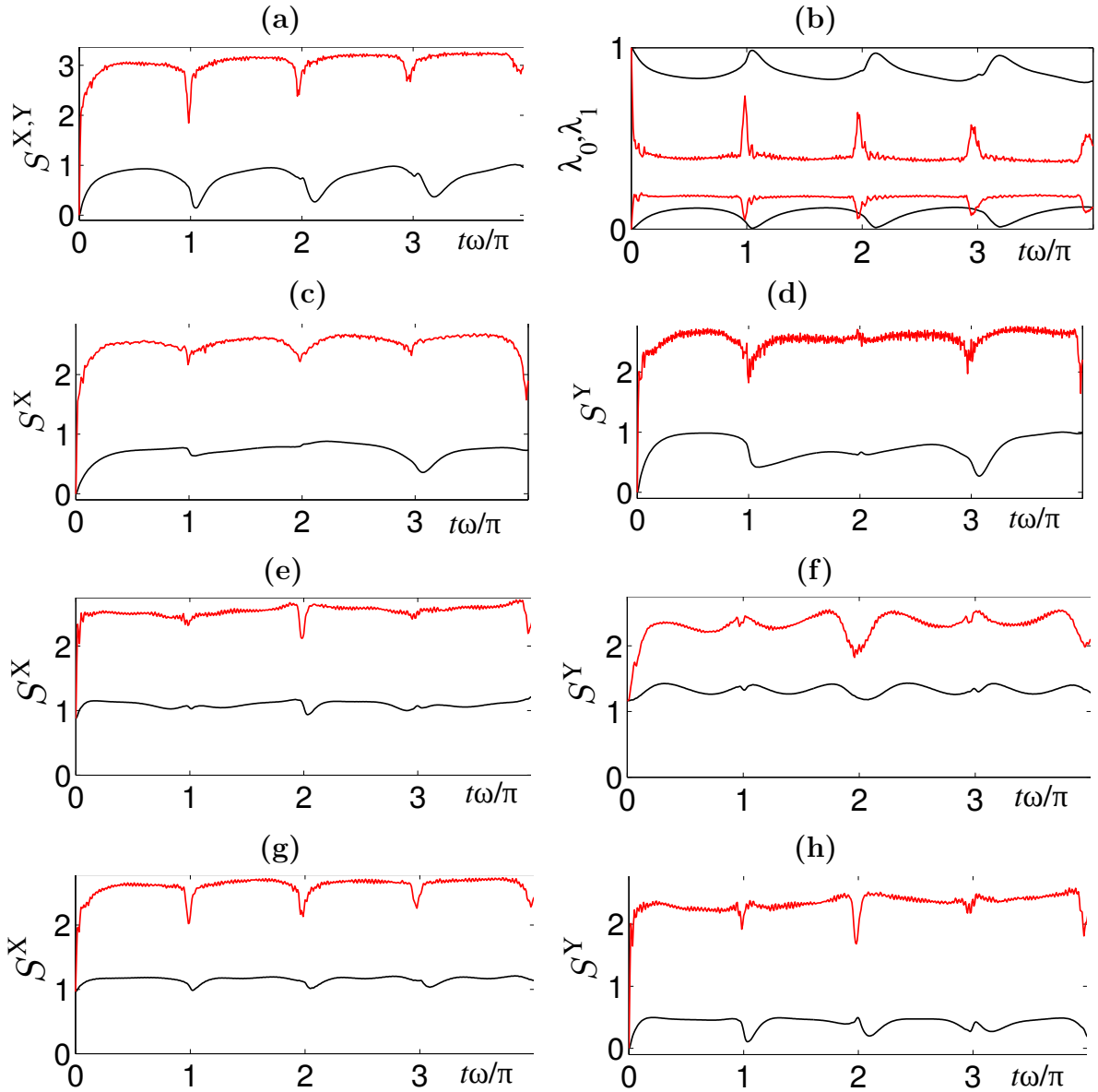

Figure 10. **(a)** Evolution of the vNE after a quench of type **A**, where g_X and g_{XY} are quenched from 0 to 2 or to 20 (black and red curve, respectively). **(b)** Occupations of the largest and second largest natural orbital as a function of time for the same quenches. Both quantities are equal for either species. **(c)** and **(d)** Entropies S^X and S^Y for $g_X = 0$ with g_{XY} quenched to 2 or 20 (black and red curves respectively) following the quenching strategy **B**. **(e)** and **(f)** Entropies S^X and S^Y following the quenching strategy **D**, where $g_{XY} = 20$ and g_X is quenched from 0 to 2 or 20 (black and red curves respectively). **(g)** and **(h)** Dynamics of S^X and S^Y following the quenching strategy **E**, where $g_X = 20$ with g_{XY} quenched from 0 to 2 or 20 (black and red curves respectively).

of the initial correlations inherent in the system, it is a more accurate reflection of the effects stemming from the quench dynamics than the vNE.

The different behaviours for each quench case are most clearly visible by looking at

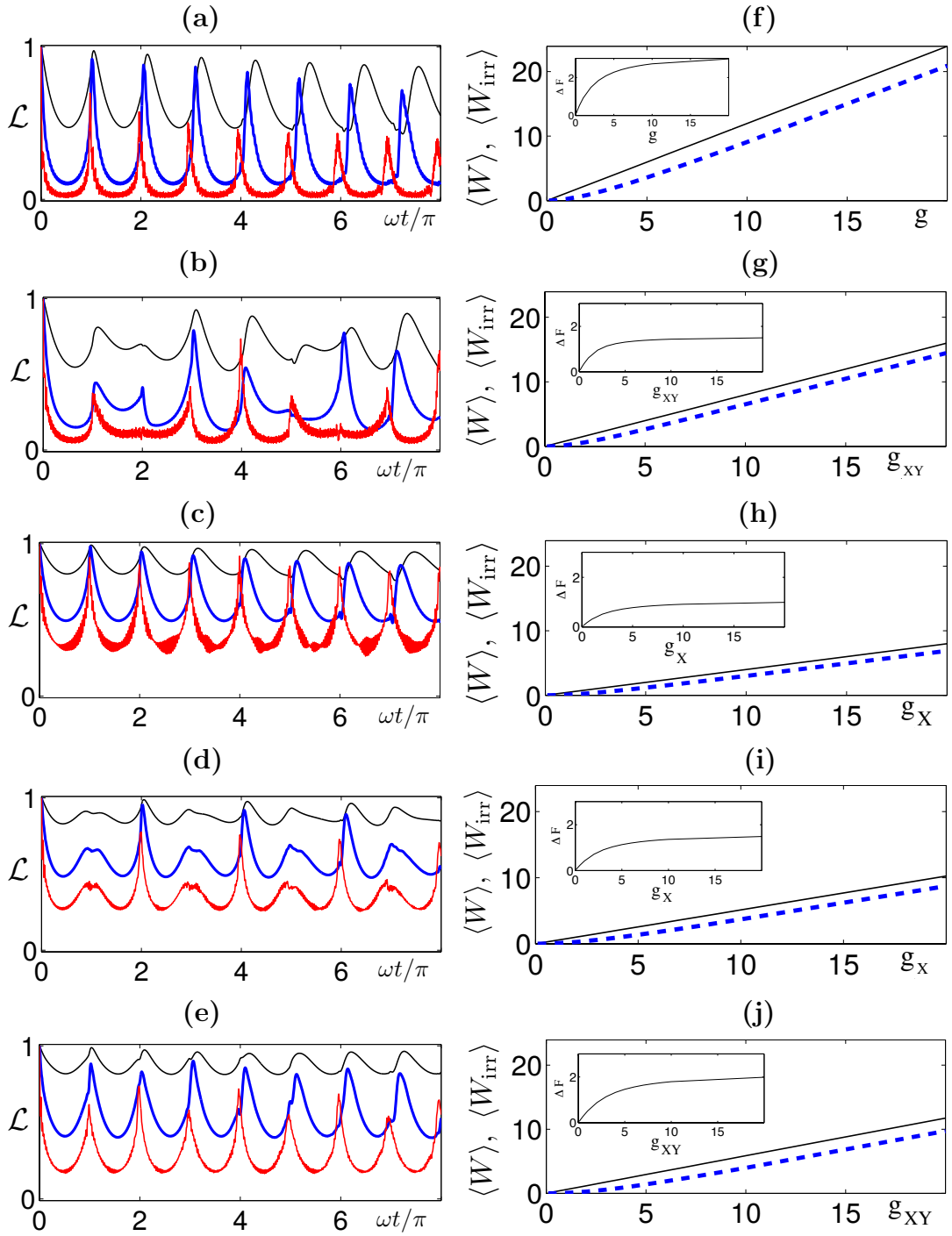

Figure 11. **(a)**-**(e)**: Temporal behavior of the LE for the different quenching strategies. **(a)** Quench **A** with $g_{\rm X} = g_{\rm XY} = 2, 6, 20$; **(b)** quench **B** with $g_{\rm XY} = 2, 6, 20$ and $g_{\rm X} = 0$; **(c)** Quench **C** with $g_{\rm X} = 2, 6, 20$ and $g_{\rm XY} = 0$; **(d)** Quench **D** with $g_{\rm X} = 2, 6, 20$ and $g_{\rm XY} = 20$; **(e)** Quench **E** with $g_{\rm XY} = 2, 6, 20$ and $g_{\rm X} = 20$. Panels **(f)** - **(j)** show the corresponding average work (solid black lines) and irreversible work (dashed blue lines) for all five quenches, with the insets showing the free energy change ΔF against the quenching amplitude.

the behaviour of the LE around the revivals. Let us first discuss quenches into the TG regime, for which the LE always displays a periodicity. For the strategies **A**, **C** and **E** the revivals have a period $\omega t/\pi$, which is due to the evolution being governed by the energy differences between the quenched states and the initial state, $\Delta E = E'_n - E_0 = q$, where q is an integer as the trapping frequencies do not change. For cases **B** and **D**, the LE is more varied and shows periodicities with $4\omega t/\pi$ and $2\omega t/\pi$. This is a consequence of the symmetry considerations discussed in Appendix A, which results in energy differences of $\Delta E = q + 1/2$ for case **D** and a combination of integer and half integer ΔE for case **B**. For weaker quenches, $g < 20$, the LEs for these two cases show rich temporal patterns which is a sign that the energy spectrum is not as degenerate as in the TG limit.

The correspondence between the LE and the characteristic function of the work distribution allows us to evaluate the average work done on the system as a result of the quench (see Figs. 11 **(f)** - **(j)**). Quite interestingly, one can see that $\langle W \rangle$ depends linearly on the quenching strength in all five scenarios. Contrarily, the irreversible work produced in these non-quasistatic processes, $\langle W_{\text{irr}} \rangle$, behaves linearly only at large values of the quench amplitude. The non-linear behaviour at small values of the quenched parameter is due to the change in the free energy ΔF (see insets of Figs. 11 **(f)** - **(j)**), which saturates for larger values of g. The latter has been calculated assuming that $\Delta F = \Delta E = E'_0 - E_0$ and taking the partition function of fictitious thermal states whose temperature has then been brought to zero.

The lower bound of the average irreversible entropy produced as a result of the quenches is shown in Fig. 12 **(a)**-**(e)** and it is apparent that $\langle \Sigma \rangle_B$ closely follows the same temporal trend as $\mathcal{L}$. This is not surprising, given that for a time-independent Hamiltonian and a system prepared in the ground state of the initial Hamiltonian, the LE coincides with the state fidelity, and the latter directly enters the definition of the Bures angle. In Fig. 12 **(f)** we show a qualitative link between the behaviour of the LE and the single particle density of the system. The visible regular dependence suggests the possibility that the behaviour of thermodynamically relevant quantities, such as the irreversible entropy production, can be inferred from experimentally accessible figures of merit such as the density profile, which we will explore in the next section.

5.3. Density evolutions

The evolution of the density profile after quench **A** for two different strengths is shown in Fig. 13 and we note that, as expected, the profiles obtained from the OBDM for X and Y are identical. One can see that the system is localised around $x = 0$ and oscillates at a frequency which depends on the strength of the quench. In fact, these oscillations mirror the appearance of the dips in the vNE and the peaks in the LE (see Figs. 10 **(a)** and 11 **(a)**). A larger amplitude of the quench leads to narrower revival peaks, which again corresponds to tighter dips (peaks) in the vNE (LE). The evolution after quenches of the form **C** and **E** is of similar form and we will therefore omit a detailed discussion here.

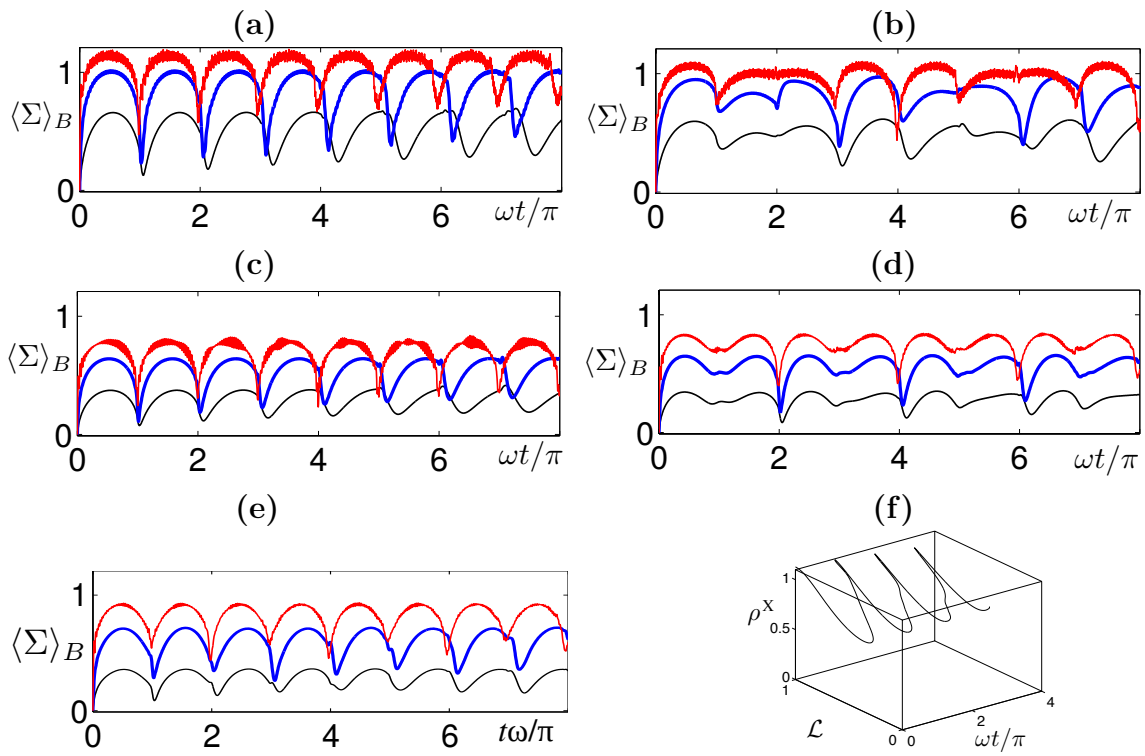

Figure 12. **(a)** - **(e)** Lower bounds of the dynamical irreversible entropies produced with the five different quenching strategies. **(a)** Quench **A** with $g_X = g_{XY} = 2, 6, 20$; **(b)** Quench **B** with $g_{XY} = 2, 6, 20$ and $g_X = 0$; **(c)** Quench **C** with $g_X = 2, 6, 20$ and $g_{XY} = 0$; **(d)** Quench **D** with $g_X = 2, 6, 20$ and $g_{XY} = 20$; **(e)** Quench **E** with $g_{XY} = 2, 6, 20$ and $g_X = 20$. In panel **(f)** the density at the centre of the trap $x = x' = 0$ of one of the atoms of species X can be seen as a function of the dimensionless time and the LE for quenching strategy **A**, with $g = 2$.

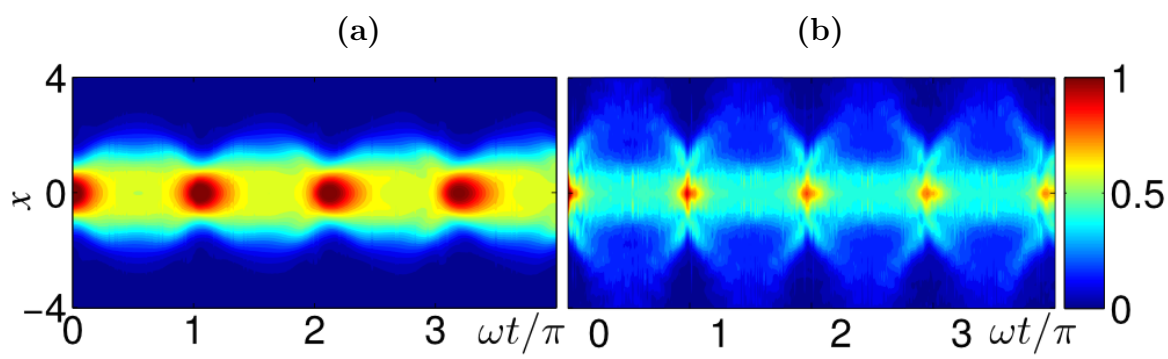

Figure 13. Evolution of the density profile $\rho^X(x)$ for a quench of strategy **A** for **(a)** $g = 2$ and **(b)** $g = 20$.

For the situation of strategy **B**, where $g_X = 0$ and g_{XY} is quenched, it is shown above that the LE and the vNE show complex dynamics for small quench values. As the two species are distinguishable in this case, we show in Fig. 14 the density evolution for an atom of species X and Y separately. For small g_{XY}, the density profile for species

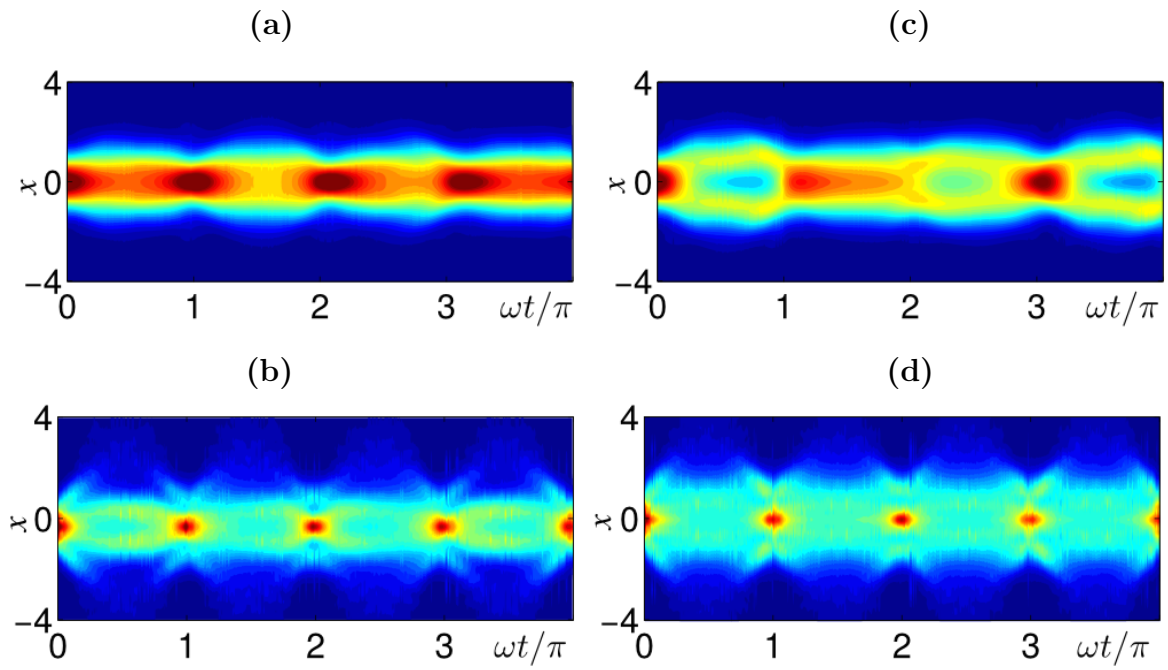

Figure 14. Density evolution of the two X atoms [**(a)** and **(b)**] and the impurity Y [**(c)** and **(d)**] for quenching strategy **B** with $g_{\rm X} = 0$ and $g_{\rm XY}$ quenched to $g = 2$ and $g = 20$ [top and bottom row of plots, respectively]. Same color-scale as in Fig. 13.

X remains localised in the center of the trap, while the impurity can *spread* to the edges of the distribution for the X atoms, forming a double peaked structure at certain times [22]. The anomalous structure of the LE in this case can be related to the irregular temporal evolution of the Y atom compared to the more periodic oscillations of the X atoms. However for larger $g_{\rm XY}$, the periodicity of the evolution becomes more regular for both species as the energy structure becomes more degenerate, resulting in complementary trends visible in the corresponding vNE and LE (see Figs. 10 **(c)** and **(d)** and 11 **(b)**).

Let us finally discuss the case of a system that is initially prepared in the ground state with strong interactions $g_{\rm XY} = 20$, which corresponds to strategy **D**. Fig. 15 shows the evolution of the density profile for a quench of $g_{\rm X}$ taken from 0 to a value that is either much smaller than $g_{\rm XY}$, or comparable to it. The phenomenology is strikingly different in this case. For $g_{\rm X} \ll g_{\rm XY}$ the density profile for the X atoms is peaked at center of the trap, while the impurity Y has a double-peak structure which is localised at the sides of the density of X. This distribution shows only a weak temporal change and the separation is maintained , which corresponds to the flat vNE of the individual species (see Fig. 10 **(e)** and **(f)**). The case in which the final value of $g_{\rm X}$ is comparable to the inter-species coupling rate shows more pronounced temporal oscillations, which are also seen in the behaviour of the vNE . The atomic species are strongly correlated regardless of the strength of the quench. However, large quenching amplitudes result in dips of the vNE at the refocusing time of the density profile that are much less pronounced than

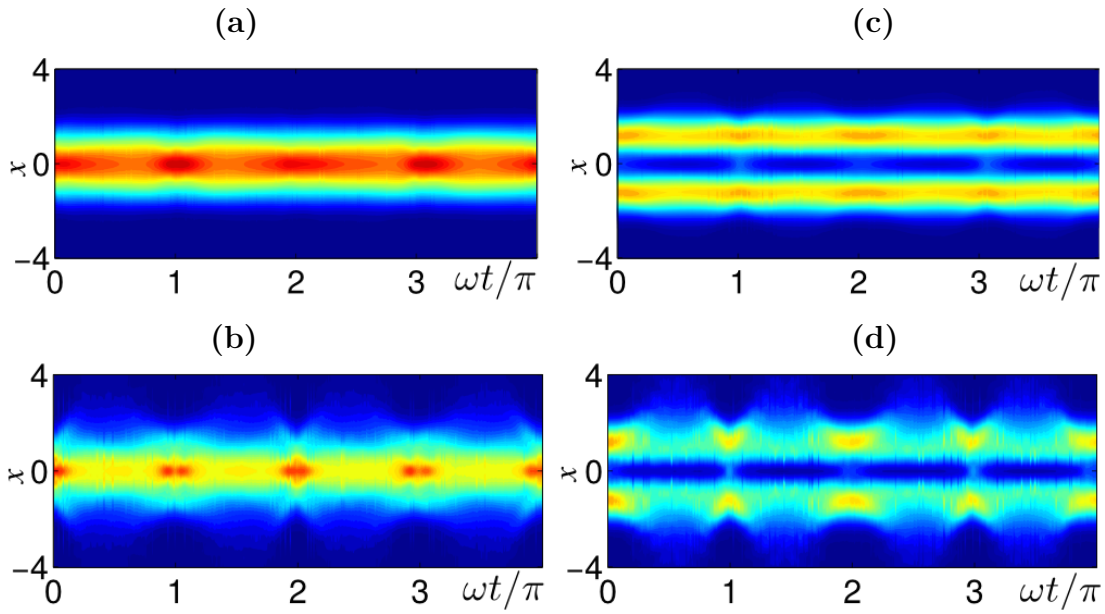

Figure 15. Evolution of the density profile for an X atom [panels **(a)** and **(b)**] and the impurity Y [panels **(c)** and **(d)**] resulting from the implementation of strategy **D**. Here $g_{\mathrm{XY}} = 20$ is constant and we consider g_{X} quenched to $g = 2$ and $g = 20$ [top and bottom row of plots, respectively]. Same color-scale as in Fig. 13.

those occurring at small final values of g_{A}. In a similar fashion, information may be also obtained from the density evolution about the structure of the LE.

A connection between the dynamics of the density profile and the evolution of thermodynamically relevant quantities would allow insight into the finite-time thermodynamics of non-equilibrium processes without requiring measurements of hard to access variables [4]. While the establishment of such a formal connection is beyond the scope of the investigation presented here, we have shown in Fig. 12 **(f)** evidence of a potential link between the LE and the density profile of our system for one example of the quenching strategies, while other complementary links may be drawn from the above discussion.

6. Conclusions

We have studied the finite-time thermodynamics of a small-sized gas of interacting bosonic particles subjected to a sudden quench of the frequency of the Hamiltonian parameters. By addressing the interplay between the quench and the mutual coupling among the constituents of the gas, we have been able to highlight the connections that finite-time thermodynamics has with relevant phenomena occurring in such few-body systems, such as the establishment of entanglement, the behaviour of the density profile, and the occurrence of orthogonality catastrophe. Notwithstanding the small number of particles involved in the system that we have addressed, the complexity of the interaction configurations (encompassing intra- and inter-species contact-like potentials) enabled a

thorough study of thermodynamically relevant figures of merit, which is well suited to pave the way to the assessment of large-size systems.

Acknowledgements

We thank Rosaria Lena, Gabriele De Chiara, and G. Massimo Palma for discussions related to the non-equilibrium thermodynamics of ultracold atomic systems. ThF, MAGM, and SC are grateful to the Okinawa Institute of Science and Technology for hospitality during the development of this project. This work was supported by the German Research Foundation (DFG, DACH project Quantum crystals of matter and light), the Okinawa Institute of Science and Technology Graduate University, the EU FP7 grant TherMiQ (Grant Agreement 618074), the John Templeton Foundation (Grant No. 43467), the UK EPSRC (EP/M003019/1). Part of this work was supported by the COST Action MP1209 "Thermodynamics in the quantum regime". M.A.G.-M. acknowledges support from EU grants OSYRIS (ERC-2013-AdG Grant No. 339106), SIQS (FP7-ICT-2011-9 No. 600645), EU STREP QUIC (H2020-FETPROACT-2014 No. 641122), EQuaM (FP7/2007-2013 Grant No. 323714), Spanish Ministry grant FOQUS (FIS2013-46768-P), the Generalitat de Catalunya project 2014 SGR 874, the John Templeton Fundation, and Fundació Cellex. Financial support from the Spanish Ministry of Economy and Competitiveness, through the "Severo Ochoa" Programme for Centres of Excellence in R&D (SEV-2015-0522) is acknowledged.

Appendix A: Degeneracies in the energy spectrum of the three-atom system

Our aim is to study the dynamics after a quench in the inter- or intra-species coupling constants over a rather large range of values. There are thus three possible final coupling configurations: (i) all the coupling constants are quenched to a non-zero value (i.e. $g_{\mathrm{X}} \in (0, \infty)$ and $g_{\mathrm{XY}} \in (0, \infty)$); (ii) only the inter-species coupling constant is quenched and the two X atoms do not interact (i.e. $g_{\mathrm{XY}} \in (0, \infty)$ and $g_{\mathrm{X}} = 0$); (iii) the interaction strength between the X atoms is quenched but the Y atom is left non-interacting (i.e. $g_{\mathrm{X}} \in (0, \infty)$ and $g_{\mathrm{XY}} = 0$).

The wave-functions in the limit $g \to \infty$ have been thoroughly discussed in the literature [26, 28, 29], and we therefore reproduce here just the ansätze which allow to accurately approximate them and become exact in the infinite limit. They are based on two facts: 1) when any of the coupling constants tend to infinity the wave function has a zero when the relative coordinate of the atoms that interact vanishes; 2) when the two atoms that interact are the two indistinguishable X atoms the wave function has a definite bosonic symmetry, and therefore the wave function cannot change sign along these zeros. On the contrary, when $g_{\mathrm{XY}} \to \infty$, a change of sign along the zeros is not forbidden, as the X and Y atoms are distinguishable.

For the first situation ($g_{\mathrm{XY}} \to \infty$ and $g_{\mathrm{X}} \to \infty$), the wave function has a zero when

$x_i - x_j$ or $x_i - y$ equal zero. In the first case, the wave function cannot change sign along this zero while in the second one the change of sign of the wave function is permitted. An ansatz accounting for the required zeros and not permitting any change of sign along them is given by

$$\Psi_1(x_1, x_2, y) \propto e^{-\frac{1}{2}(x_1^2+x_2^2+y^2)}|x_1 - x_2|\ |x_1 - y|\ |x_2 - y|, \tag{30}$$

while two other possibilities allowing for a change of sign across the $x_i - y$ zero are

$$\Psi_2(x_1, x_2, y) \propto e^{-\frac{1}{2}(x_1^2+x_2^2+y^2)}|x_1 - x_2|(x_1 - y)(x_2 - y), \tag{31}$$

$$\Psi_3(x_1, x_2, y) \propto e^{-\frac{1}{2}(x_1^2+x_2^2+y^2)}|x_1 - x_2| \times \left[(x_1 - y)\ |x_2 - y| + |x_1 - y|(x_2 - y)\right]. \tag{32}$$

All three wave functions are energetically degenerate for infinite coupling constants. However, for finite but large coupling, the wave function Ψ_1 is the ground state, and the highest excited state in this quasi-degenerate triplet is Ψ_2. The effect of the different symmetry conditions can also be seen in the energy eigenspectra the Hamiltonian (26), which we shown in Fig. 9. They are numerically calculated using an exact diagonalisation algorithm [30].

More formally, by performing the Jacobi transformation [20, 21]

$$R = \frac{1}{3}(x_1 + x_2 + y),\ S = \frac{1}{\sqrt{2}}(x_1 - x_2), T = \frac{1}{\sqrt{6}}(x_1 + x_2) - \sqrt{\frac{3}{2}}y, \tag{33}$$

the Hamiltonian Eq. (26) can be written as $\mathcal{H} = \mathcal{H}_{\rm com} + \mathcal{H}_{\rm rel} + \mathcal{V}_{\rm int}$, where

$$\mathcal{H}_{\rm com} = -\frac{1}{2}\left(\partial^2_{R^2} - R^2\right), \quad \mathcal{H}_{\rm rel} = -\frac{1}{2}\sum_{J=S,T}\left(\partial^2_{J^2} - J^2\right),$$

$$\mathcal{V}_{\rm int} \quad = g_{\rm X}\delta(S) + g_{\rm XY}\delta(-\frac{1}{2}S + \frac{\sqrt{3}}{2}T) + g_{\rm XY}\delta(-\frac{1}{2}S - \frac{\sqrt{3}}{2}T). \tag{34}$$

The $\mathcal{H}_{\rm com}$ part describes the motion of a single particle of mass $M = 3m$ with coordinate R and the relative motion of the three atoms, described by $\mathcal{H}_{\rm rel}$ and $\mathcal{V}_{\rm int}$, occurs in the plane defined by variables S and T. We consider the computational basis consisting of the eigenstates $|n_R, n_S, n_T\rangle$ of the single-particle Hamiltonian $\mathcal{H}_{\rm sp} = \mathcal{H}_{\rm com} + \mathcal{H}_{\rm rel}$. The COM motion is independent of the relative motion, so that $|n_R, n_S, n_T\rangle = |n_R\rangle \otimes |n_S, n_T\rangle$ with $|n_R\rangle$ being the eigenstates of a one-dimensional harmonic oscillator

$$\psi_{n_R}(R) = \frac{1}{\sqrt[4]{\pi}}\frac{e^{-R^2/2}}{\sqrt{2^{n_R} n_R!}}H_{n_R}(R). \tag{35}$$

For $g_{\rm XY} = g_{\rm X} = 0$ all wave functions can be written in terms of a basis of Hermite polynomials as in Ref. [22] (see also [31] where an angular basis in the $S - T$ plane is used) and the total energies are given by $E = 3/2 + n_R + n_S + n_T$, where the quantum numbers n_R and n_T can take any integer value. On the contrary n_S is restricted to even values because the wave function has to be even under the interchange of x_1 and x_2, which is equivalent to the transformation $S \to -S$. The wave functions with the same sum of $n_R + n_S + n_T$ are degenerate, and this explains the degeneracies that occur at vanishing coupling constants in Fig. 9. For $g_{\rm XY} \to \infty = g_{\rm X} \to \infty$ a triple degeneracy

in the ground state appears for large values of the coupling constants, as can be seen in Fig. 9 **(a)**. The next triplet of excited states corresponds to an excitation of the COM. In the next group some wave functions, which correspond to a second excitation of the COM, overlap with ones which correspond to an excitation of the relative motion (see Ref. [22], where only the REL energies are depicted).

The energy spectrum for three indistinguishable atoms is shown in Fig. 9 **(d)**. In such a case, there is only one coupling constant, $g_{\rm XY} = g_{\rm X} = g$, and the wave function has to be even when interchanging the Y atom with any of the two X atoms. Thus, for $g = 0$ the wave function also has to be even under this transformation, which spatially corresponds to a reflection with respect to the $S = \pm\sqrt{3}T$ axis (for all possible transformations see Refs. [20, 32]). Note that in this case n_T is no longer a good quantum number even when $g = 0$. For $g \to \infty$ wave function (30) is the non-degenerate ground state of the system. This is the completely symmetrized version of the Slater determinant which gives the solution for a system of ideal fermions, according to the Bose-Fermi mapping theorem [33, 34]. In this case the functions (31) and (32) are no longer solutions. Note that the three-indistinguishable atom energy spectra show much less degeneracies than in the 2+1 case. Also, as shown in Ref. [22], the ground state for all values of $g_{\rm XY} = g_{\rm X}$ is exactly the same for both cases.

In the situation where $g_{\rm XY} \to \infty$ and $g_{\rm X} = 0$, the wave function has to have a zero when $x_i = y$, with no specified symmetry. The ansatz for the two quasi-degenerate lowest energy states are

$$\Psi_1^{(b)}(x_1, x_2, y) \propto e^{-\frac{1}{2}(x_1^2+x_2^2+y^2)}|x_1 - y|\ |x_2 - y|, \tag{36}$$

$$\Psi_3^{(b)}(x_1, x_2, y) \propto e^{-\frac{1}{2}(x_1^2+x_2^2+y^2)}\left[(x_1 - y)\ |x_2 - y| + |x_1 - y|(x_2 - y)\right] \tag{37}$$

and the corresponding energy spectrum is shown in Fig. 9 **(b)**. For very large values of $g_{\rm XY}$ we can observe the double degeneracy of the ground state and the first excited doublet corresponds to an excitation of the COM. On the contrary, the next excited state is a singlet, which has been thoroughly discussed in Refs. [21, 22, 31].

The situation where $g_{\rm X} \to \infty$ and $g_{\rm XY} = 0$, corresponds to a system of a TG gas of 2 atoms in the presence of a non-interacting atom, and the wave function is

$$\Psi_1^{(c)}(x_1, x_2, y) \propto e^{-\frac{1}{2}(x_1^2+x_2^2+y^2)}|x_1 - x_2|. \tag{38}$$

The ground state is non-degenerate and the spectrum as a function of $g_{\rm X}$ is the sum of the spectra for two atoms, which is analytically solved in [25], and that of a non-interacting third atom (see Fig. 9 **(c)**). Note that the degeneracies present for vanishing coupling constants are lifted in different ways depending on which coupling constant is changed (see Figs. 9 **(a)**, **(b)** and **(c)**).

In the second and third situation the parameters $g_{\rm X}$ or $g_{\rm XY}$ can be increased towards infinity, and therefore move towards the first situation. The energy spectrum for varying $g_{\rm X}$ while keeping $g_{\rm XY}$ large is shown in Fig. 9 **(e)** and in this case one can identify states that do not change in energy, which was described as a non-interacting wave function in Refs. [21, 22, 31]. Finally, the energy spectrum as a function of $g_{\rm XY}$ and while $g_{\rm X}$ large is shown in Fig. 9 **(f)**, where non-interacting states can be also identified.

Appendix B: Comparison with indistinguishable atoms

It is also interesting to compare the evolution of the density, the vNE, and occupation of the natural orbitals shown in Figs. 10 and 13 with that of a system of three indistinguishable atoms. The energy spectrum for such a system is shown in Fig. 9 **(d)**, and clear differences from that of two atoms plus a third distinguishable one are visible. In the latter case triple degenerate states occur in the limit $g_{\mathrm{X}}, g_{\mathrm{XY}} \to \infty$ (see Fig. 9 **(a)**) and a discrete group theory analysis presented in Refs. [20, 22, 32, 35] showed that these three degenerate states belong to different irreducible representations of the group. The discrete group to which these solutions belong is the discrete rotational group of order 2, $\mathcal{C}^2$, restricted by the bosonic symmetry under interchange of the two indistinguishable atoms. Indeed, for all finite values of the coupling constants, all wave functions can be classified according to the possible irreducible representations of this group. In Ref. [22] it was shown that the ground state for the three indistinguishable atoms was the same as the 2+1 case for all values of $g = g_{\mathrm{X}} = g_{\mathrm{XY}}$. This is not too surprising, as these solutions obey all symmetries under interchange of two atoms required by the three-indistinguishable atoms which coincide with the ones required by the corresponding irreducible representation of the group in the 2+1 system.

By comparing the dynamical evolution of the density, the vNE, and the occupations of the natural orbitals for a system of three-indistinguishable atoms with the 2+1 setting, we find that they all coincide. The reason for this is that the initial state is a non-interacting Gaussian state with certain symmetries, which corresponds to the absence of a change in the sign of the wave function when any pair of atoms interchanges their coordinates. Therefore it belongs to a definite irreducible representation of the $\mathcal{C}^2$, restricted by the bosonic symmetry under the interchange of the two X atoms [22]. If the system has this symmetry initially, the dynamical evolution has to conserve it, so only part of the energy spectra in the 2+1 case plays a role in the evolution. This part of the energy spectra is exactly the same as in the case of three indistinguishable atoms.

References

[1] I.M. Georgescu, S. Ashhab, and F. Nori, Rev. Mod. Phys. **86**, 153 (2014).

[2] S. Trotzky, Y.-A. Chen, A. Flesch, I. P. McCulloch, U. Schollwöck, J. Eisert, and I. Bloch, Nat. Phys. **8**, 325 (2012); M. Cheneau, P. Barmettler, D. Poletti, M. Endres, P. Schauß, T. Fukuhara, C. Gross, I. Bloch, C. Kollath, and S. Kuhr, Nature **481**, 484 (2012); T. Fukuhara, A. Kantian, M. Endres, M. Cheneau, P. Schauß, S. Hild, D. Bellem, U. Schollwöck, T. Giamarchi, C. Gross, I. Bloch, and S. Kuhr, Nat. Phys. **9**, 235 (2013); T. Fukuhara, P. Schauß, M. Endres, S. Hild, M. Cheneau, I. Bloch, and C. Gross, Nature **502**, 76 (2013).

[3] M. Schreiber, S.S. Hodgman, P. Bordia, H.P. Löuschen, M.H. Fischer, R. Vosk, E. Altman, U. Schneider, and I. Bloch, Science **349**, 842 (2015).

[4] M. Campisi, P. Hänggi, and P. Talkner, Rev. Mod. Phys. **83**, 771 (2011).

[5] T.B. Batalhão, A.M. Souza, L. Mazzola, R. Auccaise, R.S. Sarthour, I.S. Oliveira, J. Goold, G. De Chiara, M. Paternostro, and R.M. Serra, Phys. Rev. Lett. **113**, 140601 (2014); T.B. Batalhão, A.M. Souza, R.S. Sarthour, I.S. Oliveira, M. Paternostro, E. Lutz, and

R.M. Serra, Phys. Rev. Lett. **115**, 190601 (2015); J.P.P. Silva, R.S. Sarthour, A.M. Souza, I.S. Oliveira, J. Goold, K. Modi, D.O. Soares-Pinto, and L.C. Celeri, arXiv:1412.6490 (2014).

[6] J. Goold, T. Fogarty, N. Lo Gullo, M. Paternostro, and Th. Busch, Phys. Rev. A **84**, 063632 (2011).

[7] A. Sindona, J. Goold, N. Lo Gullo, S. Lorenzo, and F. Plastina, Phys. Rev. Lett. **111**, 165303 (2013).

[8] S. Campbell, M.A. García-March, T. Fogarty, and Th. Busch, Phys. Rev. A **90**, 013617 (2014).

[9] R. Dorner, J. Goold, C. Cormick, M. Paternostro, and V. Vedral, Phys. Rev. Lett. **109**, 160601 (2012); L. Fusco, S. Pigeon, T.J.G. Apollaro, A. Xuereb, L. Mazzola, M. Campisi, A. Ferraro, M. Paternostro, and G. De Chiara, Phys. Rev. X **4**, 031029 (2014); T.J.G. Apollaro, G. Francica, M. Paternostro, and M. Campisi, Physica Scripta **2015**, 014023 (2015).

[10] A. Sindona, J. Goold, N. Lo Gullo, and F. Plastina, New J. Phys. **16**, 045013 (2014).

[11] R. G. Lena, G. M. Palma, and G. De Chiara, arXiv:1603.05918

[12] S. Deffner, and E. Lutz, Phys. Rev. Lett. **107**, 140404 (2011).

[13] J. Grond, A.I. Streltsov, A.U.J. Lode, K Sakmann, L.S. Cederbaum, and O.E. Alon Phys. Rev. A **88**, 023606 (2013)

[14] R. Schmitz, S. Krönke, L. Cao, and P. Schmelcher Phys. Rev. A **88**, 043601 (2013)

[15] A. Iu. Gudyma, G. E. Astrakharchik, and Mikhail B. Zvonarev Phys. Rev. A **92**, 021601(R) (2015)

[16] F. Plastina, A. Alecce, T.J.G. Apollaro, G. Falcone, G. Francica, F. Galve, N. Lo Gullo, and R. Zambrini, Phys. Rev. Lett. **113**, 260601 (2014).

[17] S. Deffner, and E. Lutz, Phys. Rev. E **77**, 021128 (2008).

[18] M. Huber, M. Perarnau-Llobet, K.V. Hovhannisyan, P. Skrzypczyk, C. Klöckl, N. Brunner, and A. Acín, New J. Phys. **17**, 065008 (2015); D.E. Bruschi, M. Perarnau-Llobet, N. Friis, K.V. Hovhannisyan, and M. Huber, Phys. Rev. E **91**, 032118 (2015).

[19] A. Carlisle, L. Mazzola, M. Campisi, J. Goold, F.L. Semio, A. Ferraro, F. Plastina, V. Vedral, G. De Chiara, and M. Paternostro, arXiv:1403.0629 (2014).

[20] N.L. Harshman, Phys. Rev. A **86**, 052122 (2012).

[21] N.T. Zinner, A.G. Volosniev, D.V. Fedorov, A.S. Jensen, and M. Valiente, Europhys. Lett. **107**, 60003 (2014).

[22] M.A. Garcia-March, B. Juliá-Díaz, G.E. Astrakharchik, J. Boronat, and A. Polls, Phys. Rev. A **90**, 063605 (2014).

[23] A. S. Dehkharghani, A. Volosniev, J. Lindgren, J. Rotureau, C. Forssen, D. Fedorov, A. Jensen and N. Zinner, Scientific Reports **5**, 10675 (2015).

[24] M.A. Garcia-March, A.S. Dehkharghani, and N.T. Zinner, J. Phys. B: At. Mol. Opt. Phys. **49**, 075303 (2016).

[25] Th. Busch, B.-G. Englert, K. Rzazewski, and M. Wilkens, Found. Phys. **28**, 549 (1998).

[26] M.D. Girardeau, and A. Minguzzi, Phys. Rev. Lett. **99**, 230402 (2007).

[27] F. Deuretzbacher, D. Becker, J. Bjerlin, S.M. Reimann, and L. Santos, Phys. Rev. A **90**, 013611 (2014).

[28] F. Deuretzbacher, K. Fredenhagen, D. Becker, K. Bongs, K. Sengstock, and D. Pfannkuche, Phys. Rev. Lett. **100**, 160405 (2008).

[29] J. Levinsen, P. Massignan, G.M. Bruun, and M.M. Parish, Science Advances **1**, e1500197 (2015).

[30] M.A. Garcia-March, and Th. Busch, Phys. Rev. A **87**, 063633 (2013).

[31] N.J.S. Loft, A.S. Dehkharghani, N.P. Mehta, A.G. Volosniev, and N.T. Zinner, Eur. Phys. J. D **69**, 65 (2015).

[32] N.L. Harshman, Few-Body Syst., **57**, 11 (2016).

[33] M. Girardeau, J. Math. Phys. **1**, 516 (1960).

[34] M.D. Girardeau, E.M. Wright, and J.M. Triscari, Phys. Rev. A **63**, 033601 (2001).

[35] V.A. Yurovsky, Phys. Rev. Lett. **113**, 200406 (2014).